

Chiral zigzag modes and flatbands in network models of twisted bilayer graphene

C. De Beule,¹ F. Dominguez,¹ and P. Recher^{1,2}

¹*Institute for Mathematical Physics, TU Braunschweig, 38106 Braunschweig, Germany*

²*Laboratory for Emerging Nanometrology, 38106 Braunschweig, Germany*

(Dated: December 22, 2024)

We construct a phenomenological scattering theory for the triangular network of valley Hall states that arises in twisted bilayer graphene under interlayer bias. Crucially, our network model includes scattering between different valley Hall states within the same valley and spin. We show that in the absence of forward scattering, the network gives rise to a nested Fermi surface or flatbands known as pseudo-Landau levels, which can be understood in terms of one-dimensional chiral zigzag modes or closed triangular orbits, respectively. Furthermore, we demonstrate how unitarity and symmetries constrain the coupling between zigzag modes leading to robust nesting.

In twisted bilayer graphene (TBG) two graphene layers are stacked with a relative twist, leading to a triangular moiré pattern of alternating stacking regions which drastically alters the electronic structure [1–3]. In recent years, TBG has garnered immense interest due to the discovery of correlated insulating phases [4, 5], superconductivity [5, 6], ferromagnetism [7], nematicity [8, 9], and strange metals [10] in magic-angle TBG.

For tiny twist angles ($\theta < 1^\circ$) the lattice of TBG relaxes into sharply defined triangular AB/BA stacking domains [11–13]. When a potential bias $\pm U$ is applied between the layers, e.g. due to an electric field normal to the layers, a local gap is opened in the AB/BA stacking regions with local valley Chern number $N_K = -N_{K'} \approx \pm \text{sgn}(U/\gamma_\perp)$ where the sign corresponds to AB or BA stacking and γ_\perp is the interlayer hopping [14]. Consequently, each valley and spin hosts two chiral modes along AB/BA domain walls that propagate in opposite directions for different valleys [14–17].

When the Fermi energy is tuned in the local gap, the low-energy excitations are entirely due to a triangular network of valley Hall states. Recently, microscopic calculations showed that the network gives rise to one-dimensional (1D) chiral zigzag modes along three independent directions related by C_3 rotation symmetry, which trivially leads to a nested Fermi surface with three C_3 -related nesting vectors [18, 19]. However, these results are inconsistent with current network theories [17] and at odds with recent transport experiments that reported interference oscillations incompatible with decoupled 1D chiral modes [20, 21]. At the moment, it is unclear how this triplet of 1D chiral zigzag modes arises from the network and how they are coupled.

In this paper, we construct a network model [22] for TBG under interlayer bias where the links of the network are given by AB/BA domain walls and the scattering nodes correspond to AA stacking regions, as shown in Fig. 1(a). We assume that the valleys are decoupled as the moiré pattern varies slowly on the interatomic scale for small twist angles, but include scattering between the two valley Hall states for a given valley and spin. While the two valley Hall states do not scatter to each other

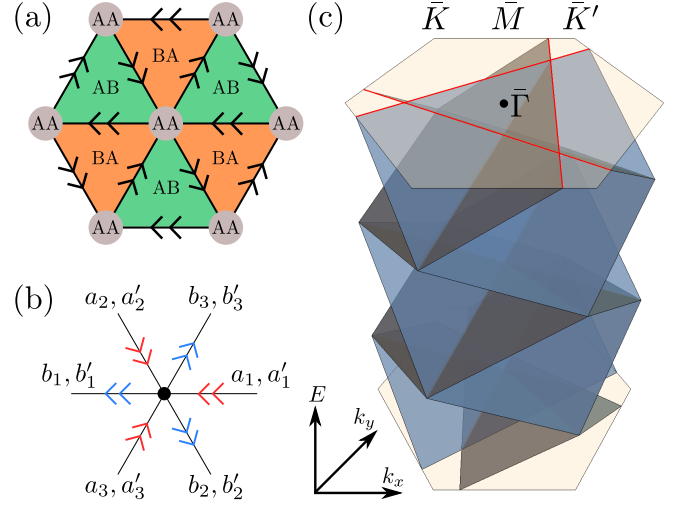


FIG. 1. (color online) (a) Stacking domains of TBG showing the network of valley Hall states (for a single valley and spin) that emerges upon applying an interlayer bias. AB/BA domain walls and AA regions correspond to the links and scattering nodes of the network model, respectively. (b) Unit cell of the network. (c) Network spectrum for K valley in the moiré Brillouin zone for the case with no forward scattering and $\phi = 0$ [see Eq. (5)]. Due to the 1D nature of the network eigenmodes, the Fermi surface (red lines) is nested.

along the links in the absence of disorder, it is not *a priori* clear why the valley Hall states remain decoupled when they reach the AA stacking regions where the local gap induced by the interlayer bias vanishes.

Taking into account the symmetries of TBG under interlayer bias and unitarity, we show that in the absence of forward scattering, our network model generically gives rise to a triplet of quasi 1D chiral modes as well as flatbands known as pseudo-Landau levels. These regimes differ in the relative phase acquired after a 120° deflection between the two valley Hall states. We also show that the robust Fermi surface nesting [18, 19] can be understood in terms of a suppression of forward scattering due to the geometry of the network combined with symmetry constraints and unitarity.

Network model — We consider a network with two chiral modes along each link which scatter at nodes that form a triangular lattice, as illustrated in Fig. 1(a). The unit cell of this triangular chiral network is shown in Fig. 1(b). Each scattering node has six incoming and six outgoing modes. We label the nodes by their position vector $\mathbf{r}_{ij} = i\mathbf{l}_1 + j\mathbf{l}_2$ where $\mathbf{l}_{1,2} = l(-1/2, \pm\sqrt{3}/2)$ are the moiré lattice vectors with $l = a/2 \sin(\theta/2)$ the moiré lattice constant and where a is the lattice constant of graphene. Incoming modes are denoted as $a_{ij} = (a_{1,ij}, a_{2,ij}, a_{3,ij})$ and a'_{ij} for the two chiral channels, while outgoing modes are denoted as b_{ij} and b'_{ij} , such that $(b, b')^t = \mathcal{S}(a, a')^t$ with \mathcal{S} the S -matrix relating incoming to outgoing modes.

To constrain the S -matrix, we take into account the symmetries of TBG under interlayer bias. At small twist angles, the symmetries of TBG become independent of the twist center [23, 24] so that we do not have to consider a specific lattice realization. Symmetries that preserve the valley are given by C_3 and C_2T , where T is (spinless) time-reversal symmetry and C_3 and C_2 are rotations by $2\pi/3$ and π about the z -axis with respect to the center of an AA region, respectively. Note that C_2 exchanges A and B sublattices and valleys. These symmetries impose the following conditions on the S -matrix [25]:

$$C_3 : \quad \mathcal{S} = C_3 \mathcal{S} C_3^{-1}, \quad (1)$$

$$C_2 : \quad \mathcal{S}_{K'} = \mathcal{S}_K, \quad (2)$$

$$T : \quad \mathcal{S}_{K'} = (\mathcal{S}_K)^t, \quad (3)$$

$$C_2T : \quad \mathcal{S} = \mathcal{S}^t, \quad (4)$$

where C_3 corresponds to a cyclic permutation of the incoming modes $(a_1, a'_1) \rightarrow (a_2, a'_2) \rightarrow (a_3, a'_3) \rightarrow (a_1, a'_1)$ and similar for outgoing modes.

To proceed, we first neglect forward scattering, which is a good starting point as the wave-function overlap between incoming and outgoing modes is larger for deflections than for forward scattering, simply due to the geometry of the triangular network [26]. In contrast to previous network models for TBG under interlayer bias [17], we take into account scattering at the nodes (AA regions) between the two chiral modes belonging to the same valley and spin. The most general S -matrix that obeys C_3 and C_2T in the absence of forward scattering is given in the supplemental material [25]. If we further assume that interchannel deflections to the left and right are equal, the S -matrix can be written as

$$\mathcal{S} = \frac{e^{i\varphi}}{2} \begin{pmatrix} S_{\phi, \phi} & S_{0, \pi} \\ S_{\pi, 0} & -S_{-\phi, -\phi} \end{pmatrix}, \quad (5)$$

with

$$S_{\vartheta, \psi} = \begin{pmatrix} 0 & e^{i\vartheta} & e^{i\psi} \\ e^{i\psi} & 0 & e^{i\vartheta} \\ e^{i\vartheta} & e^{i\psi} & 0 \end{pmatrix}, \quad (6)$$

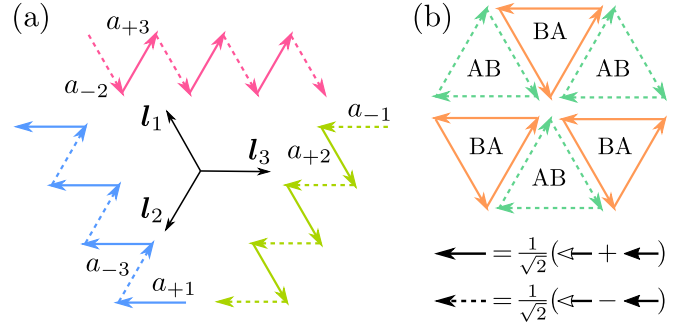


FIG. 2. (color online) (a) Triplet of 1D chiral zigzag modes for $\phi = 0$ along directions \mathbf{l}_j ($j = 1, 2, 3$) with $\mathbf{l}_3 = -(\mathbf{l}_1 + \mathbf{l}_2)$, where solid (dashed) lines are (anti)symmetric superpositions of valley Hall states along the same link $a_{\pm} = (a \pm a')/\sqrt{2}$. (b) Localized network for $\phi = \pi/2$ and illustration of superpositions of a and a' (solid and open arrowheads).

with real phases φ and ϕ . Using Bloch's theorem, we relate the incoming modes to the outgoing modes of the same node, $(a, a')^t = e^{iEl/\hbar v} [\mathbf{1}_2 \otimes \mathcal{M}(\mathbf{k})] (b, b')^t$ where $e^{iEl/\hbar v}$ is the dynamical phase accumulated along a link with v the velocity of the chiral modes, which we assume is equal for the two valley Hall states, and $\mathcal{M}(\mathbf{k}) = \text{diag}(e^{ik_3}, e^{ik_1}, e^{ik_2})$ with $k_j = \mathbf{k} \cdot \mathbf{l}_j$ ($j = 1, 2, 3$) and $\mathbf{l}_3 = -(\mathbf{l}_1 + \mathbf{l}_2)$. The network energy bands are then found from $\det(\mathbf{1}_6 - e^{iEl/\hbar v} [\mathbf{1}_2 \otimes \mathcal{M}(\mathbf{k})] \mathcal{S}) = 0$ [17, 27].

The phase ϕ in \mathcal{S} determines the interference between the network modes and appear as phenomenological parameters. In reality, they depend on system parameters such as the Fermi energy, the interlayer bias, twist angle, etc.. However, by inspection we find that when $\phi = 0$, the network spectrum is given by

$$E_{j,n}(\mathbf{k}) = \frac{\hbar v}{2l} (2\pi n - \varphi + k_j), \quad (7)$$

where $n \in \mathbb{Z}$ and which is shown in Fig. 1(c). In this case, the network spectrum is periodic in energy with period $\pi\hbar v/l$ and $E_{i,n}(\mathbf{k} + \mathbf{g}) = E_{i,n+m}(\mathbf{k})$ with \mathbf{g} a moiré reciprocal lattice vector and m an integer. To gain some insight, we perform a unitary transformation $U = [\mathbf{1}_6 + i\sigma_y e^{i\phi\sigma_z} \otimes \mathbf{1}_3]/\sqrt{2}$ on the scattering matrix, which corresponds to changing the original basis a, a' to a basis of symmetric and antisymmetric superpositions (SAS) of valley Hall states on the same link $a_{\pm} = (a \pm a')/\sqrt{2}$ and similar for outgoing modes. In the SAS basis, there are only interchannel deflections [25] that proceed in clockwise (counterclockwise) fashion for a_+ (a_-) as illustrated in Fig. 2(a), giving rise to three independent 1D chiral zigzag channels [19]. Owing to their linear dispersion, the density of states of the 1D zigzag modes is constant and given by $2\sqrt{3}/\pi\hbar vl$, such that each band with bandwidth $\hbar v\pi/l$ hosts one electron per moiré unit cell (for each valley and spin).

Another special case is given by $\phi = \pi/2$, which results in three doubly-degenerate flatbands per energy period

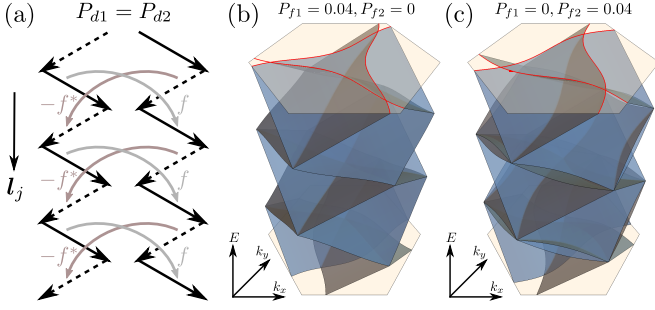


FIG. 3. Effects of forward scattering on the zigzag network with $P_{d1} = P_{d2}$. (a) Coupling mechanism between parallel zigzag channels along \mathbf{l}_j ($j = 1, 2, 3$). (b) Network spectrum for $P_{f1} = 0.04$ and $P_{f2} = 0$ and (c) $P_{f1} = 0$ and $P_{f2} = 0.04$.

$\hbar v 2\pi/l$, given by ($j = 0, 1, 2$)

$$E_{j,n}(\mathbf{k}) = \frac{\hbar v}{l} \left(2\pi n - \varphi + \frac{2\pi}{3} j \right), \quad (8)$$

that we identify with pseudo-Landau levels [28]. In the SAS basis, there are now only intrachannel deflections, such that a_+ (a_-) modes perform counterclockwise (clockwise) orbits around BA (AB) domains as shown in Fig. 2(b). Hence, the network modes are localized, leading to flatbands. Because the orbits consist of superpositions of two chiral modes with different momenta, we expect a non-trivial standing wave pattern to arise [28].

We thus find that in the absence of forward scattering, depending on the phase ϕ in Eq. (5), the network gives rise to 1D chiral zigzag modes or flatbands. These two regimes are consistent with microscopic calculations [18, 19]. Moreover, this shows that the pseudo-Landau levels can also be understood from the chiral network.

Chiral zigzag modes — We now explore the effect of forward scattering between the valley Hall states on the chiral zigzag modes ($\phi = 0$). For concreteness, we consider $\varphi = 0$ and allow for intra- and interchannel forward scattering with probabilities P_{f1} and P_{f2} . We also allow for different intra- and interchannel deflection probabilities P_{d1} and P_{d2} . Here, we further assume that the intrachannel probabilities P_{f1} and P_{d1} are equal for the two valley Hall states. In this case, current conservation requires $2(P_{d1} + P_{d2}) + P_{f1} + P_{f2} = 1$, and we can take

$$P_{f1} = (\sin \alpha_1 \sin \alpha_2)^2, \quad P_{f2} = (\sin \alpha_1 \cos \alpha_2)^2, \quad (9)$$

$$P_{d1} = \frac{1}{2}(\cos \alpha_1 \cos \alpha_3)^2, \quad P_{d2} = \frac{1}{2}(\cos \alpha_1 \sin \alpha_3)^2, \quad (10)$$

with $\alpha_{1,2,3} \in [0, \pi/2]$. The corresponding S -matrix is given in the supplemental material [25]. We find

$$U^\dagger S U = \begin{pmatrix} f \mathbb{1}_3 & S \\ S^\dagger & -f^* \mathbb{1}_3 \end{pmatrix}, \quad (11)$$

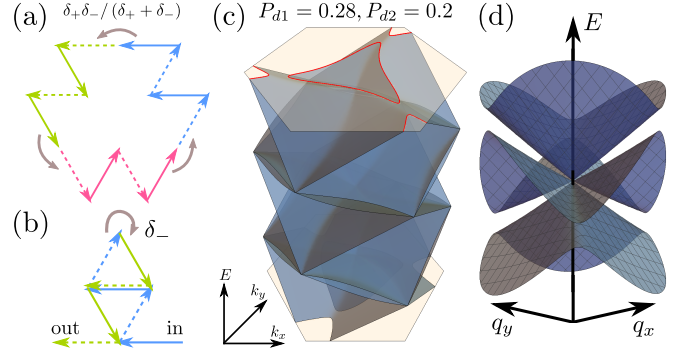


FIG. 4. (color online) (a,b) Couplings between different zigzag modes which arise due to $P_{d1} \neq P_{d2}$. (c) Network spectrum for $P_{f1} = P_{f2} = 0.02$, $P_{d1} = 0.28$, and $P_{d2} = 0.2$. (d) Zoom of (c) near \bar{K} with $\mathbf{q} = \mathbf{k} - \bar{K}$.

where $f = \sqrt{P_{f2}} + i\sqrt{P_{f1}} \sin \chi$,

$$S = \frac{-\delta_+ \delta_-}{\delta_+ + \delta_-} \mathbb{1}_3 + \begin{pmatrix} 0 & \delta_+ & \delta_- \\ \delta_- & 0 & \delta_+ \\ \delta_+ & \delta_- & 0 \end{pmatrix}, \quad (12)$$

with $\delta_\pm = \frac{\sqrt{P_{d1}} \pm \sqrt{P_{d2}}}{2\sqrt{P_{f1}P_{d1}}}$, and $\cos \chi = (P_{d2} - P_{d1})/2\sqrt{P_{f1}P_{d1}}$. Note that S is only well-defined if χ is real, i.e. $2\sqrt{P_{f1}P_{d1}} \geq |P_{d2} - P_{d1}|$.

First, we consider $P_{d1} = P_{d2}$ for which $\delta_- = 0$ and $\chi = \pi/2$. We find that in this case only parallel zigzag channels are coupled due to intrachannel forward scattering in the SAS basis with probability $|f|^2$, which is illustrated in Fig. 3(a). The network spectrum is now given by ($j = 1, 2, 3$)

$$E_{j,\pm,n}(\mathbf{k}) = \frac{\hbar v}{l} \left[2\pi n - i \log \frac{1}{2} \left(F_j(\mathbf{k}) \pm \sqrt{4e^{ik_j} + F_j(\mathbf{k})^2} \right) \right], \quad (13)$$

where $F_j(\mathbf{k}) = f^* e^{-ik_{j+1}} - f e^{-ik_{j+2}}$ with j defined cyclically and which is shown in Figs. 3(b) and (c). As expected, coupling between parallel zigzag channels does not lead to anti-crossings and only warps the Fermi surface. Interestingly, the shape of the Fermi surface depends on the type of forward scattering. For $P_{f2} = 0$, we find that the network bands are symmetric about k_y as in this case $F_1(k_x, -k_y) = F_2(k_x, k_y)$ and $F_3(k_x, -k_y) = F_3(k_x, k_y)$. Furthermore, states at the $\bar{\Gamma}$, \bar{K} , and \bar{K}' points in the network Brillouin zone remain triply degenerate, but are shifted in energy as $F_j(0) = -2i\sqrt{P_{f1}}$ and $F_j(\pm\bar{K}) = \pm 2e^{\pm i\pi/6}\sqrt{P_{f1}}$ for all j .

In general, we see from Eq. (12) that the three zigzag channels are coupled through two processes, which are illustrated in Figs. 4(a) and (b). One process is due to interchannel forward scattering in the SAS basis with probability $[\delta_+ \delta_- / (\delta_+ + \delta_-)]^2$ [see Fig. 4(a)], while the other

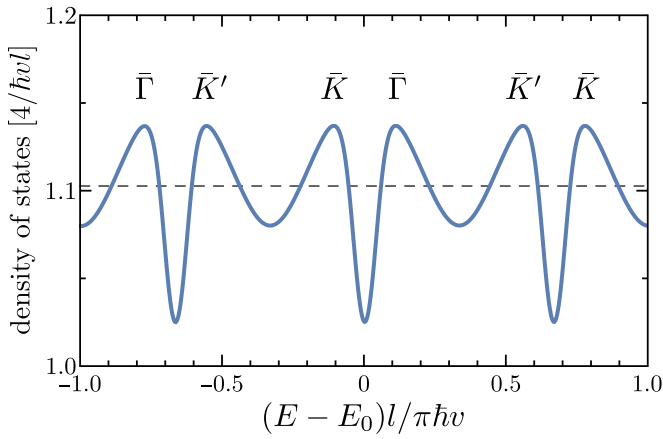


FIG. 5. DOS over one energy period $2\pi\hbar v/l$ of the spectrum shown in Fig. 4(c). The dashed line gives the constant DOS when the zigzag modes are decoupled ($P_{d1} = P_{d2}$) corresponding to the spectra in Figs. 1(c) and 3(b) and (c). Maxima in the DOS are due to crossings at high-symmetry points in the moiré Brillouin zone as indicated on the figure.

is due to clockwise (counterclockwise) deflections from antisymmetric (symmetric) to symmetric (antisymmetric) superpositions of valley Hall states with probability δ_-^2 [see Fig. 4(b)]. Both processes lead to anti-crossings in the network spectrum as shown in Fig. 4(c). In this case, there are no analytical solutions. Nevertheless, we find numerically that the network hosts quasi Dirac cones near $\bar{\Gamma}$ and $\pm\bar{K}$, as shown in Fig. 4(d). These nodes give rise to maxima in the density of states (DOS) which is shown in Fig. 5. Minima in the DOS correspond to energies where the anti-crossing due to coupling of different zigzag modes is largest, which occurs at energies in between the nodes at $\bar{\Gamma}$ and $\pm\bar{K}$ [25].

With these results, we can understand the robustness of the Fermi surface nesting reported in Ref. 18. Firstly, due to the geometry of the triangular network, forward scattering is suppressed as the wave-function overlap between incoming and outgoing modes is relatively smaller for forward scattering than deflections [26]. Secondly, when forward scattering is small ($\alpha_1 \approx 0$), unitarity enforces $\delta_- \approx 0$, and therefore coupling between the three different zigzag channels is suppressed. This is shown in Fig. 6, where we show $|\delta_-|$ for (α_1, α_3) consistent with C_3 , C_2T , and unitarity, i.e. when $2\sqrt{P_{f1}P_{d1}} \geq |P_{d2} - P_{d1}|$, for $\alpha_2 = \pi/2$ ($P_{f2} = 0$). Reducing α_2 shrinks the allowed area in the (α_1, α_3) -plane, which in the figure corresponds to the area enclosed by the gray-scaled curves and the right-vertical axis [25].

Conclusions — We have constructed a phenomenological scattering theory for the triangular network of valley Hall states, which arises at low-energies in twisted bilayer graphene under interlayer bias. Our model is based solely on the symmetries of twisted bilayer graphene and unitarity of the S -matrix. In the absence of forward scat-

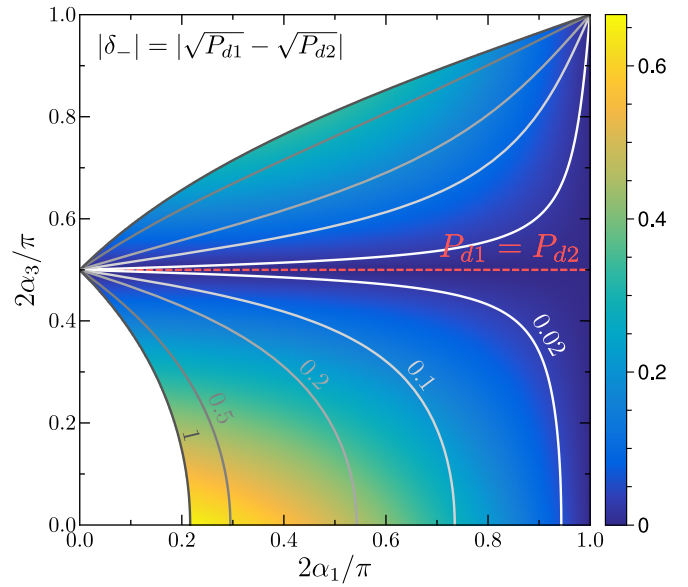


FIG. 6. (color online) $|\delta_-| = |\sqrt{P_{d1}} - \sqrt{P_{d2}}|$ in the (α_1, α_3) -plane where white regions are incompatible with symmetries and unitarity for any value of α_2 . The area enclosed by the gray-scaled curves and the right-vertical axis correspond to allowed (α_1, α_3) for given $2\alpha_2/\pi$ as denoted next to the curves.

tering, the network model gives rise to a nested Fermi surface and pseudo-Landau levels, simply by tuning the phases picked up after 120° deflections. In this sense, we give a unified explanation of these two phenomena, both arising from the network, in terms of one-dimensional chiral zigzag modes and closed triangular orbits in the basis of symmetric and antisymmetric superpositions of valley Hall states. Furthermore, we have explored the effect of forward scattering between the valley Hall states on the chiral zigzag modes. In particular, we have shown that the robustness of the nesting arises due to the geometry of the triangular network, which suppresses forward scattering and conspires with symmetry and unitarity such that the three zigzag channels remain largely decoupled. The network model has a rich phenomenology but is simple enough at the same time to allow for qualitative predictions. Our results have important implications on electronic transport in the network regime, such as the nature of interference oscillations in recent experiments [20, 21].

Acknowledgments — F.D. and P.R. gratefully acknowledge funding by the Deutsche Forschungsgemeinschaft (DFG, German Research Foundation) within the framework of Germany's Excellence Strategy – EXC-2123 QuantumFrontiers – 390837967.

-
- [1] J. M. B. Lopes dos Santos, N. M. R. Peres, and A. H. Castro Neto, *Phys. Rev. Lett.* **99**, 256802 (2007).

- [2] R. Bistritzer and A. H. MacDonald, *Proc. Natl. Acad. Sci.* **108**, 12233 (2011).
- [3] G. Li, A. Luican, J. M. B. Lopes dos Santos, A. H. Castro Neto, A. Reina, J. Kong, and E. Y. Andrei, *Nat. Phys.* **6**, 109 (2010).
- [4] K. Kim, A. DaSilva, S. Huang, B. Fallahazad, S. Larentis, T. Taniguchi, K. Watanabe, B. J. LeRoy, A. H. MacDonald, and E. Tutuc, *Proc. Natl. Acad. Sci.* **114**, 3364 (2017).
- [5] Y. Cao, V. Fatemi, S. Fang, K. Watanabe, T. Taniguchi, E. Kaxiras, and P. Jarillo-Herrero, *Nature* **556**, 43 (2018).
- [6] M. Yankowitz, S. Chen, H. Polshyn, Y. Zhang, K. Watanabe, T. Taniguchi, D. Graf, A. F. Young, and C. R. Dean, *Science* **363**, 1059 (2019).
- [7] A. L. Sharpe, E. J. Fox, A. W. Barnard, J. Finney, K. Watanabe, T. Taniguchi, M. A. Kastner, and D. Goldhaber-Gordon, *Science* **365**, 605 (2019).
- [8] A. Kerelsky, L. J. McGilly, D. M. Kennes, L. Xian, M. Yankowitz, S. Chen, K. Watanabe, T. Taniguchi, J. Hone, C. Dean, A. Rubio, and A. N. Pasupathy, *Nature* **572**, 95 (2019).
- [9] Y. Choi, J. Kemmer, Y. Peng, A. Thomson, H. Arora, R. Polski, Y. Zhang, H. Ren, J. Alicea, G. Refael, F. von Oppen, K. Watanabe, T. Taniguchi, and S. Nadj-Perge, *Nat. Phys.* **15**, 1174 (2019).
- [10] Y. Cao, D. Chowdhury, D. Rodan-Legrain, O. Rubies-Bigordà, K. Watanabe, T. Taniguchi, T. Senthil, and P. Jarillo-Herrero, *Phys. Rev. Lett.* **124**, 76801 (2020).
- [11] N. N. T. Nam and M. Koshino, *Phys. Rev. B* **96**, 075311 (2017).
- [12] H. Yoo, R. Engelke, S. Carr, S. Fang, K. Zhang, P. Cazeaux, S. H. Sung, R. Hovden, A. W. Tsen, T. Taniguchi, K. Watanabe, G.-C. Yi, M. Kim, M. Luskin, E. B. Tadmor, E. Kaxiras, and P. Kim, *Nat. Mater.* **18**, 448 (2019).
- [13] N. R. Walet and F. Guinea, *2D Mater.* **7**, 015023 (2019).
- [14] F. Zhang, A. H. MacDonald, and E. J. Mele, *Proc. Natl. Acad. Sci.* **110**, 10546 (2013).
- [15] I. Martin, Y. M. Blanter, and A. F. Morpurgo, *Phys. Rev. Lett.* **100**, 036804 (2008).
- [16] P. San-Jose and E. Prada, *Phys. Rev. B* **88**, 121408(R) (2013).
- [17] D. K. Efimkin and A. H. MacDonald, *Phys. Rev. B* **98**, 035404 (2018).
- [18] M. Fleischmann, R. Gupta, F. Wulfschläger, S. Theil, D. Weckbecker, V. Meded, S. Sharma, B. Meyer, and S. Shallcross, *Nano Lett.* **20**, 971 (2020).
- [19] B. Tsim, N. N. T. Nam, and M. Koshino, arXiv:2001.06257.
- [20] P. Rickhaus, J. Wallbank, S. Slizovskiy, R. Pisoni, H. Overweg, Y. Lee, M. Eich, M.-H. Liu, K. Watanabe, T. Taniguchi, T. Ihn, and K. Ensslin, *Nano Lett.* **18**, 6725 (2018).
- [21] S. G. Xu, A. I. Berdyugin, P. Kumaravadivel, F. Guinea, R. Krishna Kumar, D. A. Bandurin, S. V. Morozov, W. Kuang, B. Tsim, S. Liu, J. H. Edgar, I. V. Grigorieva, V. I. Fal'ko, M. Kim, and A. K. Geim, *Nat. Commun.* **10**, 3 (2019).
- [22] J. T. Chalker and P. D. Coddington, *J. Phys. C Solid State Phys.* **21**, 2665 (1988).
- [23] H. C. Po, L. Zou, A. Vishwanath, and T. Senthil, *Phys. Rev. X* **8**, 031089 (2018).
- [24] L. Zou, H. C. Po, A. Vishwanath, and T. Senthil, *Phys. Rev. B* **98**, 085435 (2018).
- [25] See supplemental material [url to be added].
- [26] Z. Qiao, J. Jung, C. Lin, Y. Ren, A. H. MacDonald, and Q. Niu, *Phys. Rev. Lett.* **112**, 206601 (2014).
- [27] H. K. Pal, S. Spitz, and M. Kindermann, *Phys. Rev. Lett.* **123**, 186402 (2019).
- [28] A. Ramires and J. L. Lado, *Phys. Rev. Lett.* **121**, 146801 (2018).

Supplemental Material

S1. SYMMETRY CONSTRAINTS ON THE S-MATRIX

First, we consider C_3 rotation symmetry which preserves the valley. We find that

$$\mathcal{S} = C_3 \mathcal{S} C_3^{-1}, \quad (1)$$

where C_3 is a cyclic permutation $(a_1, a'_1) \rightarrow (a_2, a'_2) \rightarrow (a_3, a'_3) \rightarrow (a_1, a'_1)$ of the incoming modes as defined in Fig. 1(b) of the main text, and similar for outgoing modes. Next, we discuss the effect of C_2 rotation symmetry and time-reversal symmetry T . As these symmetries do not conserve the valley, we need to consider both valleys

$$\begin{pmatrix} b_K \\ b_{K'} \end{pmatrix} = \begin{pmatrix} \mathcal{S}_K & 0 \\ 0 & \mathcal{S}_{K'} \end{pmatrix} \begin{pmatrix} a_K \\ a_{K'} \end{pmatrix}. \quad (2)$$

Under C_2 rotation symmetry, we have

$$\begin{pmatrix} b_{K'} \\ b_K \end{pmatrix} = \begin{pmatrix} \mathcal{S}_K & 0 \\ 0 & \mathcal{S}_{K'} \end{pmatrix} \begin{pmatrix} a_{K'} \\ a_K \end{pmatrix}, \quad (3)$$

such that $\mathcal{S}_{K'} = \mathcal{S}_K$. On the other hand, under time-reversal symmetry we have

$$\begin{pmatrix} a_{K'}^* \\ a_K^* \end{pmatrix} = \begin{pmatrix} \mathcal{S}_K & 0 \\ 0 & \mathcal{S}_{K'} \end{pmatrix} \begin{pmatrix} b_{K'}^* \\ b_K^* \end{pmatrix}, \quad (4)$$

such that $\mathcal{S}_{K'} = (\mathcal{S}_K)^t$. Hence, the combination $C_2 T$ enforces $\mathcal{S}_K = (\mathcal{S}_K)^t$ and $\mathcal{S}_{K'} = (\mathcal{S}_{K'})^t$.

S2. S-MATRIX WITHOUT FORWARD SCATTERING

The S -matrix relates valley Hall states that propagate along AB/BA domain walls at the scattering nodes (AA regions) such that $(b, b')^t = \mathcal{S}(a, a')^t$ with a, a' six incoming modes and b, b' six outgoing modes where the prime distinguishes the two valley Hall states. In the absence of forward scattering, the most general S -matrix that is consistent with unitarity and C_3 and $C_2 T$ symmetry is given by

$$\mathcal{S} = e^{i\varphi} \begin{pmatrix} 0 & \frac{e^{i\phi} \cos \beta_1}{\sqrt{2}} & \frac{e^{i\phi} \cos \beta_1}{\sqrt{2}} & 0 & \sin \beta_1 \cos \beta_2 & \sin \beta_1 \sin \beta_2 \\ \frac{e^{i\phi} \cos \beta_1}{\sqrt{2}} & 0 & \frac{e^{i\phi} \cos \beta_1}{\sqrt{2}} & \sin \beta_1 \sin \beta_2 & 0 & \sin \beta_1 \cos \beta_2 \\ \frac{e^{i\phi} \cos \beta_1}{\sqrt{2}} & \frac{e^{i\phi} \cos \beta_1}{\sqrt{2}} & 0 & \sin \beta_1 \cos \beta_2 & \sin \beta_1 \sin \beta_2 & 0 \\ 0 & \sin \beta_1 \sin \beta_2 & \sin \beta_1 \cos \beta_2 & 0 & -\frac{e^{i\phi} \cos \beta_1}{\sqrt{2}} & -\frac{e^{i\phi} \cos \beta_1}{\sqrt{2}} \\ \sin \beta_1 \cos \beta_2 & 0 & \sin \beta_1 \sin \beta_2 & -\frac{e^{i\phi} \cos \beta_1}{\sqrt{2}} & 0 & -\frac{e^{i\phi} \cos \beta_1}{\sqrt{2}} \\ \sin \beta_1 \sin \beta_2 & \sin \beta_1 \cos \beta_2 & 0 & -\frac{e^{i\phi} \cos \beta_1}{\sqrt{2}} & -\frac{e^{i\phi} \cos \beta_1}{\sqrt{2}} & 0 \end{pmatrix}, \quad (5)$$

with φ and ϕ real phases, $\beta_2 = [\arcsin(\cot^2 \beta_1) - \pi]/2$, and $\pi/4 \leq \beta_1 \leq \pi/2$. In the main text, we consider the case $\beta_1 = \beta_2 = \pi/4$ for which the left and right interchannel deflection amplitudes are equal, which is a reasonable assumption. In this case, we find

$$U^\dagger \mathcal{S} U = \frac{e^{i\varphi}}{2} \begin{bmatrix} i \sin \phi \tilde{S} & e^{-i\phi} \cos \phi S \\ e^{i\phi} \cos \phi S^t & i \sin \phi \tilde{S}^t \end{bmatrix}, \quad S = \begin{pmatrix} 0 & 1 & 0 \\ 0 & 0 & 1 \\ 1 & 0 & 0 \end{pmatrix}, \quad \tilde{S} = \begin{pmatrix} 0 & 0 & 1 \\ 1 & 0 & 0 \\ 0 & 1 & 0 \end{pmatrix}. \quad (6)$$

where $U = [\mathbb{1}_6 + i\sigma_y e^{i\phi\sigma_z} \otimes \mathbb{1}_3]/\sqrt{2}$ is a unitary transformation that transforms $a, a' \rightarrow a_\pm = (a \pm a' e^{\mp i\phi})/\sqrt{2}$ and similar for outgoing modes b, b' . For $\phi = n\pi$ ($n \in \mathbb{Z}$),

$$U^\dagger \mathcal{S} U = (-1)^n \frac{e^{i\varphi}}{2} \begin{pmatrix} 0 & S \\ S^t & 0 \end{pmatrix}, \quad (7)$$

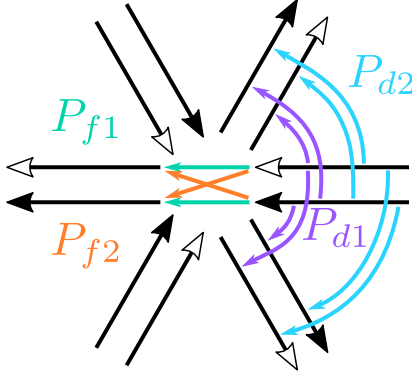


FIG. S1. Scattering processes for the S -matrix in Eq. (9) and their probabilities.

such that scattering modes form three independent chiral zigzag channels in the new basis. On the other hand, for $\phi = (n + 1/2)\pi$ ($n \in \mathbb{Z}$),

$$U^\dagger S U = (-1)^n \frac{ie^{i\varphi}}{2} \begin{pmatrix} \tilde{S} & 0 \\ 0 & \tilde{S}^t \end{pmatrix}, \quad (8)$$

such that scattering modes perform closed orbits around AB and BA domains in the new basis.

S3. GENERAL S-MATRIX FOR CHIRAL ZIGZAG REGIME

When we allow for forward scattering in the chiral zigzag regime ($\phi = 0$), the S -matrix can be written as

$$S = e^{i\varphi} \begin{pmatrix} e^{i\chi} \sqrt{P_{f1}} & \sqrt{P_{d1}} & \sqrt{P_{d1}} & -\sqrt{P_{f2}} & \sqrt{P_{d2}} & -\sqrt{P_{d2}} \\ \sqrt{P_{d1}} & e^{i\chi} \sqrt{P_{f1}} & \sqrt{P_{d1}} & -\sqrt{P_{d2}} & -\sqrt{P_{f2}} & \sqrt{P_{d2}} \\ \sqrt{P_{d1}} & \sqrt{P_{d1}} & e^{i\chi} \sqrt{P_{f1}} & \sqrt{P_{d2}} & -\sqrt{P_{d2}} & -\sqrt{P_{f2}} \\ -\sqrt{P_{f2}} & -\sqrt{P_{d2}} & \sqrt{P_{d2}} & -e^{-i\chi} \sqrt{P_{f1}} & -\sqrt{P_{d1}} & -\sqrt{P_{d1}} \\ \sqrt{P_{d2}} & -\sqrt{P_{f2}} & -\sqrt{P_{d2}} & -\sqrt{P_{d1}} & -e^{-i\chi} \sqrt{P_{f1}} & -\sqrt{P_{d1}} \\ -\sqrt{P_{d2}} & \sqrt{P_{d2}} & -\sqrt{P_{f2}} & -\sqrt{P_{d1}} & -\sqrt{P_{d1}} & -e^{-i\chi} \sqrt{P_{f1}} \end{pmatrix}, \quad (9)$$

with $\cos \chi = (P_{d2} - P_{d1}) / 2\sqrt{P_{f1}P_{d1}}$ such that χ is real, which corresponds to the condition $2\sqrt{P_{f1}P_{d1}} \geq |P_{d2} - P_{d1}|$. Here, we assumed that the probability for intrachannel processes is the same for the two valley Hall states and that the probability for left and right interchannel deflections is equal. Current conservation then requires $2(P_{d1} + P_{d2}) + P_{f1} + P_{f2} = 1$, where P_{f1} (P_{d1}) and P_{f2} (P_{d2}) are the probabilities for intra- and interchannel forward scattering (deflections), respectively, as illustrated in Fig. S1. We take the parameterization

$$P_{f1} = (\sin \alpha_1 \sin \alpha_2)^2, \quad P_{f2} = (\sin \alpha_1 \cos \alpha_2)^2, \quad P_{d1} = \frac{1}{2}(\cos \alpha_1 \cos \alpha_3)^2, \quad P_{d2} = \frac{1}{2}(\cos \alpha_1 \sin \alpha_3)^2, \quad (10)$$

with $\alpha_{1,2,3} \in [0, \pi/2]$ under the condition that χ is real, which is graphically represented in Fig. S2.

We find that when the chiral zigzag modes are coupled ($P_{d1} \neq P_{d2}$) there appear quasi Dirac cones in the network bands, as show in Fig. S2.

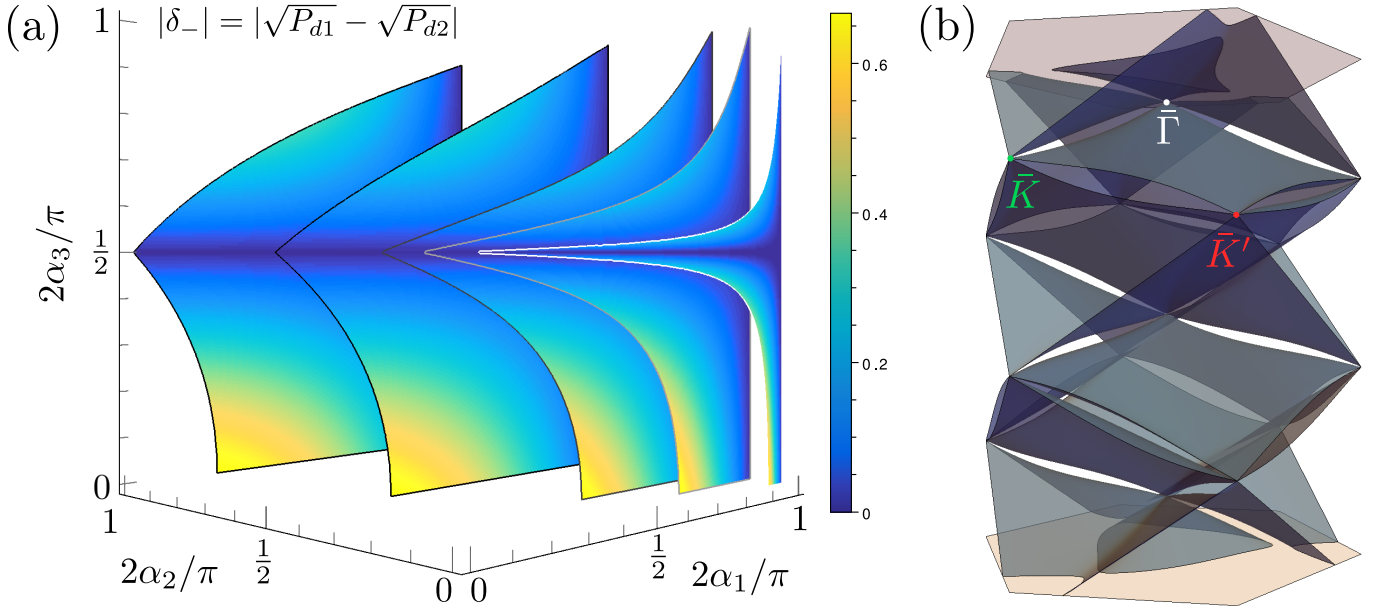


FIG. S2. (color online) (a) $|\delta_-| = |\sqrt{P_{d1}} - \sqrt{P_{d2}}|$ plotted over (α_1, α_3) regions compatible with C_3 and C_2T symmetry and unitarity of the S -matrix (real χ) for the same α_2 values as shown in Fig. 5 of the main text. (b) Network spectrum for $P_{f1} = P_{f2} = 0.02$, $P_{d1} = 0.28$, and $P_{d2} = 0.2$ [see Fig. 4(c) and (d) in the main text], showing quasi Dirac nodes at the $\bar{\Gamma}$ (white), \bar{K} (green), and \bar{K}' (red) points of the moiré Brillouin zone.